TECTONOPHYSICS

Tectonophysics 314 (1999) 401–422

www.elsevier.com/locate/tecto

Exhumation of the Danubian nappes system (South Carpathians) during the Early Tertiary: inferences from kinematic and paleostress analysis at the Getic/Danubian nappes contact

Liviu Matenco [a,*], Stefan Schmid [b]

[a] *University of Bucharest, Faculty of Geology and Geophysics, 6 Traian Vuia str., sect. 1, 70139 Bucharest, Romania*
[b] *Geologisch–Palaeontologisches Institut, Bernoullistr. 32, 4056 Basel, Switzerland*

Received 11 February 1999; accepted for publication 13 August 1999

Abstract

A detailed kinematic study based on the analysis of brittle structures, combined with a description of structures in the adjacent foredeep, allows for the definition of three major tectonic episodes during the Late Cretaceous–Tertiary evolution of the central part of the South Carpathians. Following Middle Cretaceous and older orogenic phases, the first tectonic event that affected the studied area was a Late Cretaceous NNW–SSE oriented contraction, which led to the final major emplacement of the Danubian and Getic nappes. During the Paleogene–Early Miocene, an extension event induced rapid exhumation of the Danubian units, leading to the formation of large normal faults dipping towards both the foreland and the hinterland. This extension, together with dextral rotation of the South Carpathians around the western corner of the Moesian platform, allows for the NE-ward movement of the internal continental blocks with respect to the foreland platforms. In the Late Miocene, E-ward translation of the internal South Carpathians units with respect to the Moesian Platform was accommodated through a large-scale E–W oriented strike–slip corridor within the South Carpathians. The general Paleogene–Early Miocene NE to E-ward rotation and the Late Miocene E-ward translation of the Rhodopian fragment allowed for the accommodation of roll-back and contraction taking place in the East Carpathians. © 1999 Elsevier Science B.V. All rights reserved.

Keywords: Kinematics; Metamorphic core complexes; South Carpathians; Strike–slip faults

1. Introduction

The arcuate Romanian segment of the Carpathians results from Tertiary NE to E-ward rotation of the Inner Carpathians (i.e. the Median Dacides according to Sandulescu, 1988, or the Rhodopian fragment according to Burchfiel, 1976). The Inner Carpathians consist of all tectonic units of more internal origin than the Severin/Ceahlau nappes, Danubian nappes, and the Moldavides), which invaded a pre-existent embayment of oceanic and/or thinned continental crust in the Eurasian plate (Sandulescu, 1984, 1988). The South Carpathians (Fig. 1) represent an important segment of the Carpathian loop and stretch from the oroclinal bend situated in western Romania and eastern Serbia in the west to the arcuate junction zone with the East Carpathians in the east.

* Corresponding author. Tel.: +40-1-211-7390; Fax: +40-1-211-3120.
E-mail address: matl@gg.unibuc.ro (L. Matenco)

PII: S0040-1951(99)00221-8

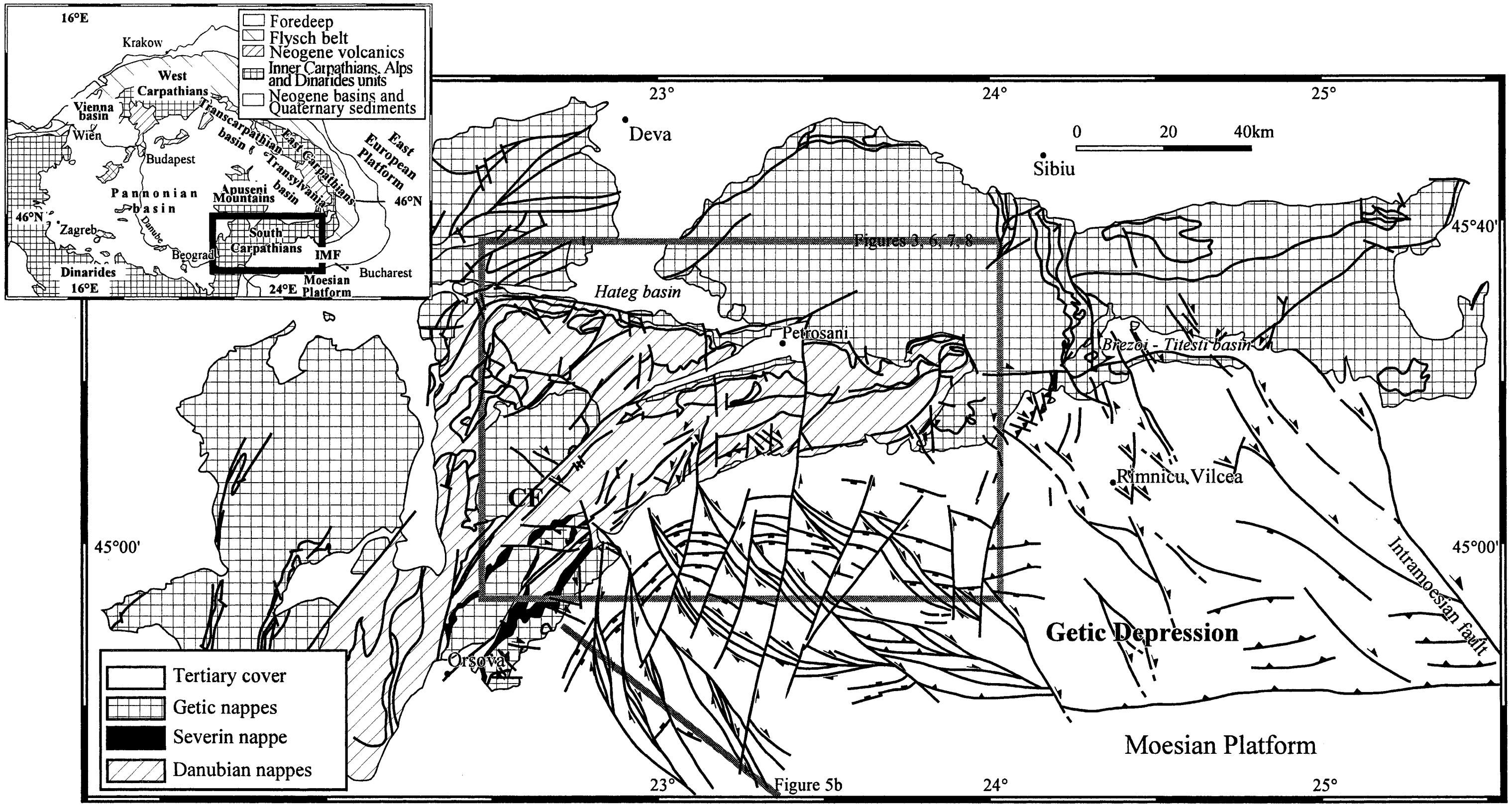

Fig. 1. Structural sketch map of the South Carpathians and of the adjacent foredeep. South Carpathians map modified after Berza et al. (1994), foredeep structural map after Matenco et al. (1997a,b) and Rabagia and Matenco (1999). Inset represents the tectonic sketch map of the Carpathians system with the location of the studied area (after Sandulescu, 1984). Rectangle represents the location of Figs. 3, 6, 7, 8; CF: Cerna fault. Note that all the foredeep faults are depicted through seismic interpretation (after Rabagia and Matenco, 1999), being covered below the Pliocene sediments of the Getic Depression.

The South Carpathians are made up of a nappe pile of basement and Mesozoic units, already formed during the Cretaceous and covered by Late Cretaceous to Tertiary post-tectonic sediments (Sandulescu, 1984; Berza et al., 1994 and references cited therein). Tertiary tectonics overprinted this nappe pile and led to foredeep sedimentation and subsurface deformation within the Getic Depression (South Carpathians foredeep) to the south (e.g. Matenco et al., 1997a,b). Traditionally (e.g. Sandulescu, 1984, 1988), the Alpine evolution is subdivided into a Triassic to Early Cretaceous extensional period, two Cretaceous (Austrian and Laramic) phases of nappe emplacement, followed by a contractional phase of Miocene age. Recently it was proposed that Early Tertiary deformation led to orogen-parallel extension (Schmid et al., 1998), pre-dating Miocene dextral wrenching between the Transylvanian basin to the north and the Moesian platform in the south (e.g. Ratschbacher et al., 1993; Matenco et al., 1997a,b).

A large number of studies focused on the architecture of the pile of basement and cover nappes in the South Carpathians (e.g. Murgoci, 1912; Streckeisen, 1934; Codarcea, 1940; Berza et al., 1983; Balintoni et al., 1989 and references cited therein). However, kinematic and dynamic studies, inferring movement directions within the internal nappes, are rare (Ratschbacher et al., 1993; Schmid et al., 1998). There was also a lack of timing constraints other than stratigraphical evidence. A combined structural and fission track study (Schmid et al., 1998) revealed Eocene to Oligocene large-scale orogen-parallel extension affecting the previously formed nappe stack of Danubian units, including the oceanic Severin unit and the sole of the Getic nappe. This previously undetected extension modifies the classical tectonic interpretation of the South Carpathians and gives new indications for the regional eastward escape of the Inner Carpathians units during the Early Tertiary. Whether or not large-scale extension also affected the Getic nappes represents a key point in establishing the kinematics and the late stage evolution of the South Carpathians. Additionally, a large-scale extensional episode, taking place at the northern margin of the South Carpathians foredeep (Matenco et al., 1997a,b; Rabagia and Matenco, 1999), well documented for Early Miocene times but possibly starting in the Paleogene, asks for an orogen-wide correlation of Tertiary deformation events within the South Carpathians mountain belt. Our study investigates whether regional-scale uplift and exhumation of the Danubian unit with respect to its margins to the north (Getic nappes and Transylvanian basin) and the south (South Carpathians foredeep) could be related to a mechanism similar to metamorphic core complex formation.

In this study we document kinematic and paleostress data collected in the South Carpathians, in order to relate ductile extensional structures described by Schmid et al. (1998) within the Danubian nappes to brittle structures particularly developed in the Getic nappes. We will also relate these structures to brittle deformations observed in the southern part of the nappe stack, and particularly to the well-dated foredeep deformations, in order to constrain the Tertiary tectonic evolution of the Getic and Danubian units in the South Carpathians.

2. Geological and tectonic settings

The studied area comprises the three major tectonic units of the South Carpathians, namely the Getic–Supragetic, Severin and Danubian nappe systems. Together with the frontal foredeep they will be briefly described below (Fig. 2).

2.1. The Getic nappes

The Getic nappes, including the so-called Supragetic nappes, represent the highest structural units of the South Carpathians and are part of the Rhodopian continental fragment (sensu Burchfiel, 1976). These nappes, also referred to as Median Dacides, can be correlated with the Bucovinian nappe system of the Central East Carpathians (Sandulescu, 1975, 1984). They comprise a pre-Alpine basement and its sedimentary cover (Late Paleozoic to Lower Cretaceous sequence of conglomerates, quartzitic sandstones, shales and limestones). The pre-Alpine basement consists of older medium to high-grade metamorphic units, low-

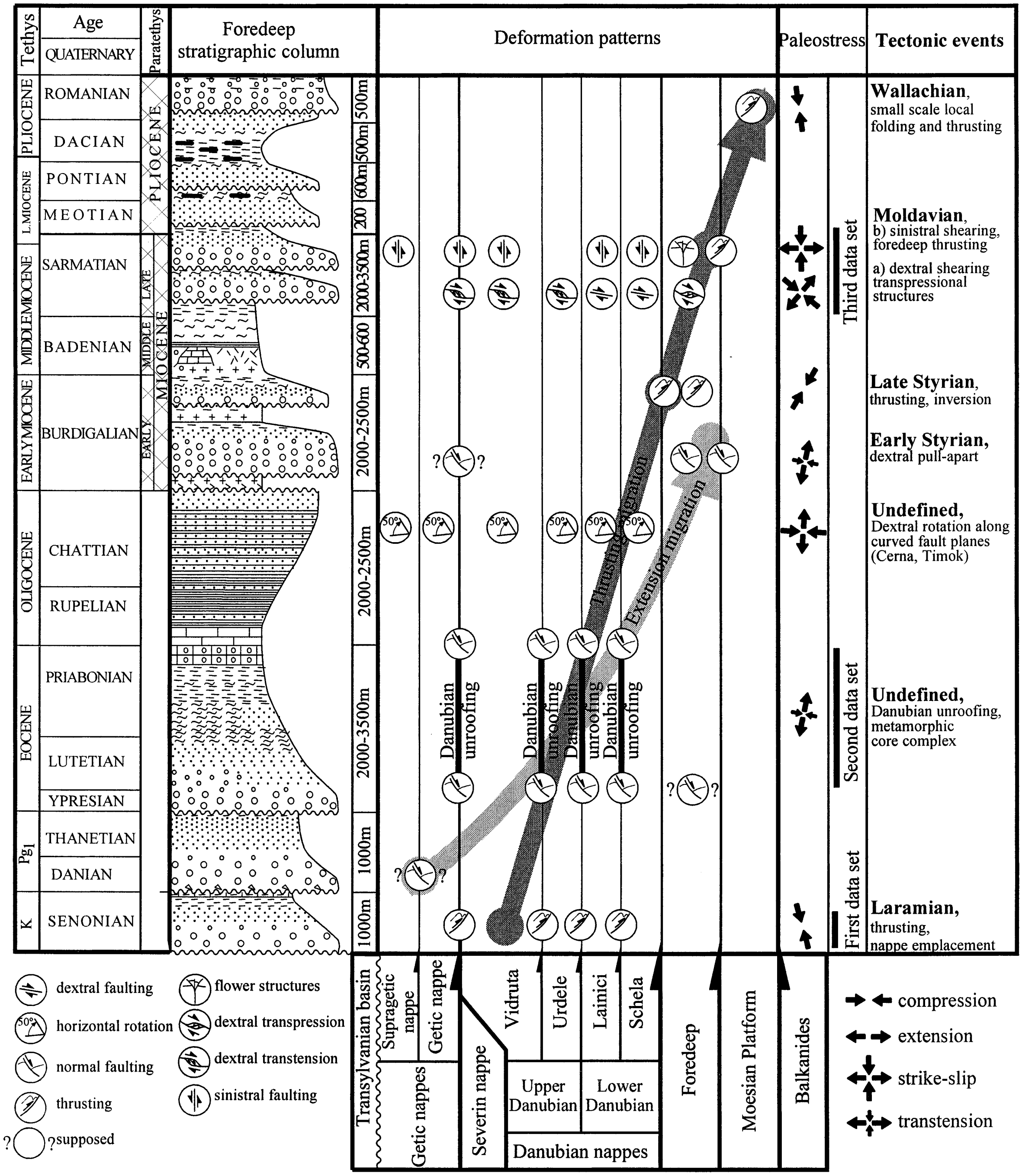

Fig. 2. Stratigraphic correlation and tectonic evolution scheme of the South Carpathians for the Uppermost Cretaceous–Tertiary with the structural results of the present study and correlation with the tectonic episodes defined by Matenco et al. (1997a,b), Schmid et al. (1998) and Rabagia and Matenco (1999) (correlation of Tethys–Paratethys after Rögl, 1996). Note the differences in the Miocene–Pliocene between the Tethys and the local Paratethys stages used in the present study. Grey arrows represent an attempt to define regional extensional and thrusting migration patterns in a foreland-breaking sequence. Foredeep sedimentological cycles are defined after Dicea (1995), Rabagia and Matenco (1999), and our own results. The dark grey arrow represents the general foreland thrusting migration, while the light grey arrow represents the proposed foreland extensional migration pattern.

grade Paleozoic sequences (Cambrian–Silurian and Upper Devonian–Lower Carboniferous metasedimentary rocks and related magmatites), and Upper Paleozoic coal-bearing, coarse sedimentary deposits of molasse type and scarce magmatic rocks (Iancu and Maruntiu, 1994). This basement is intruded by Paleozoic granitoids of 310–350 Ma (Stan et al., 1992 in Iancu and Maruntiu, 1994).

The major Alpine deformation within the Getic and Supragetic thrust sheets took place during the Middle Cretaceous ('Austrian phase') (Codarcea, 1940; Sandulescu, 1984, 1988; Berza et al., 1994). The Severin deposits were deformed in an acretionary wedge setting and partially overridden by the Getic crystalline during Neocomian to Aptian times (Bojar et al., 1998). The Getic nappes are primarily exposed in the hinterland of the South Carpathians but they also form klippen in the frontal part of the South Carpathians, thrusted on top of the Danubian nappes (Godeanu, Valari, Portile de Fier, Bahna) during a later ('Laramian', i.e. Late Cretaceous) episode (Figs. 1 and 3).

2.2. The Severin nappe

The Severin nappe comprises ophiolitic slices and Cretaceous flysch units, derived from a thinned continental and oceanic realm situated between the Rhodopian fragment and the Moesian (European) platform. They form the continuation of similar units found in the East Carpathians (e.g. Sinaia flysch) and can be traced into the oroclinal bend between the South Carpathians and Balkan mountains (e.g. Berza et al., 1994). The Severin nappe, already sealed to the Getic realm during the Middle Cretaceous phase, was thrust onto the

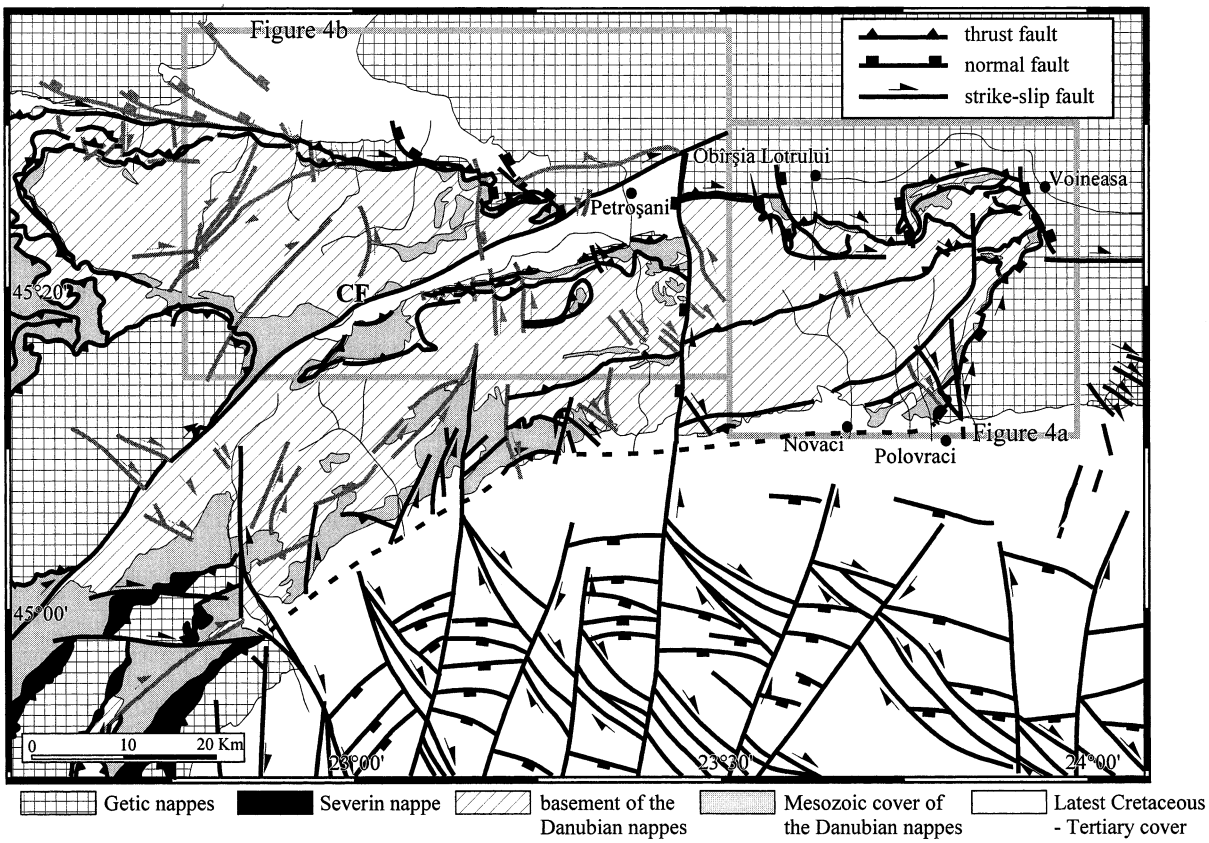

Fig. 3. Structural map of the central–eastern Danubian units with the structures active during the Latest Cretaceous–Tertiary (modified after Berza et al., 1994). Squared areas represent insets for Fig. 4A and B; CF: Cerna fault. Foredeep faults convention as in Fig. 1.

Danubian nappes during the Late Cretaceous Laramian episode. The Severin nappe was severely stretched and dismembered due to this overthrusting of the Getic–Supragetic over the Danubian thrust sheets (Codarcea, 1940; Burchfiel, 1976; Sandulescu, 1984; Berza et al., 1994).

2.3. The Danubian nappes

Paleogeographically, the Danubian nappes (Figs. 2 and 3) represent the most external thick-skinned units of the South Carpathians mountains. The Danubian thrust sheets (see Berza et al., 1983, 1994; Berza and Draganescu, 1988; Sandulescu, 1984 and references cited therein for a complete description) were described in terms of a large-scale antiformal stack formed between a roof thrust (sole of the Getic/Severin nappes) and a floor thrust above the Moesian platform (Seghedi and Berza, 1994), from which the nappes have probably been peeled off already during the Late Cretaceous, being finally emplaced during the Middle Miocene (Stefanescu et al., 1988) (Figs. 2, 4 and 5A). According to fission track ages (Schmid et al., 1998; Bojar et al., 1998), final exhumation of the Danubian units took place during the Eocene to Early Miocene, when large-scale orogen-parallel extension partly accommodated the NE to E-ward movement of the Rhodopian fragment. The Danubian units formed a core complex (Schmid et al., 1998) exhumed along a major detachment fault (Getic detachment) (Fig. 5A). According to subsurface information (Getic Depression), the Danubian nappes later overrode Miocene sediments of the Moesian foreland, Pliocene sediments onlapping onto Danubian and Getic units (Matenco et al., 1997a,b) (Fig. 5B). Note that an alternative interpretation by Bojar et al. (1998) suggests a Latest Cretaceous age for the onset of core complex formation in the Retezat area (NW Danubian), shortly post-dating Late Campanian–Early Maastrichtian Danubian crustal thickening. However, their apatite cooling ages in the Danubian units are mostly Paleogene to Early Miocene in age, 2 to 4 km having been removed during this time span in order to exhume the Danubian basement (Bojar et al., 1998). The internal structure of the thrust sheets, formed during the Late Cretaceous thrusting, relies on the individualisation of two major nappe systems: the Upper Danubian nappes (Vidruta, Urdele and local equivalents) which discontinuously outcrop along the belt, and the Lower Danubian nappes (Lainici, Schela) which have a larger regional extent (Berza et al., 1994) (Fig. 5A).

The basement of the Danubian thrust sheets comprises high-grade metamorphic rocks of pre-Cambrian age (e.g. Berza and Iancu, 1994; Liegois et al., 1997 and references cited therein), often penetratively overprinted by lower greenschist facies mylonitisation during Variscan and Alpine deformations (Berza et al., 1994; Dallmeyer et al., 1998; Schmid et al., 1998). The metamorphic grade of Paleozoic series does not exceed lower greenschist facies conditions. The Mesozoic sedimentary cover comprises Lower Jurassic continental deposits followed by Upper Jurassic to Lower Cretaceous platform carbonates, Albian to Turonian pelagic limestones and Late Cretaceous terrigeneous flysch. Areas with Alpine lower greenschist facies metamorphism of the Mesozoic cover are restricted to the northeastern and northern part of the Danubian window (Ciulavu and Ferreiro-Mählmann, 1999).

2.4. Intramontane Tertiary basins and South Carpathians foredeep

The deformed part of the southern foredeep (namely the Getic Depression) represents the most external unit of the South Carpathians belt, comprising more than 6 km of molasse type Tertiary sediments (e.g. Fig. 5B). Following Late Cretaceous and older orogenic phases the foredeep was first affected by Paleogene?–Early Miocene large-scale dextral transtension responsible for the opening of the Getic Depression as a pull-apart basin (Rabagia and Fülop, 1994; Matenco et al., 1997a,b; Matenco, 1997; Rabagia and Matenco, 1999). Subsequent Middle Miocene contraction produced WNW–ESE striking thrusts and associated syntectonic sedimentation developed in piggy-back basins. The last tectonic episode relates to general transpression during the Late Miocene–Early Pliocene: a first set of NW–SE oriented dextral shears is displaced by N–S oriented sinistral

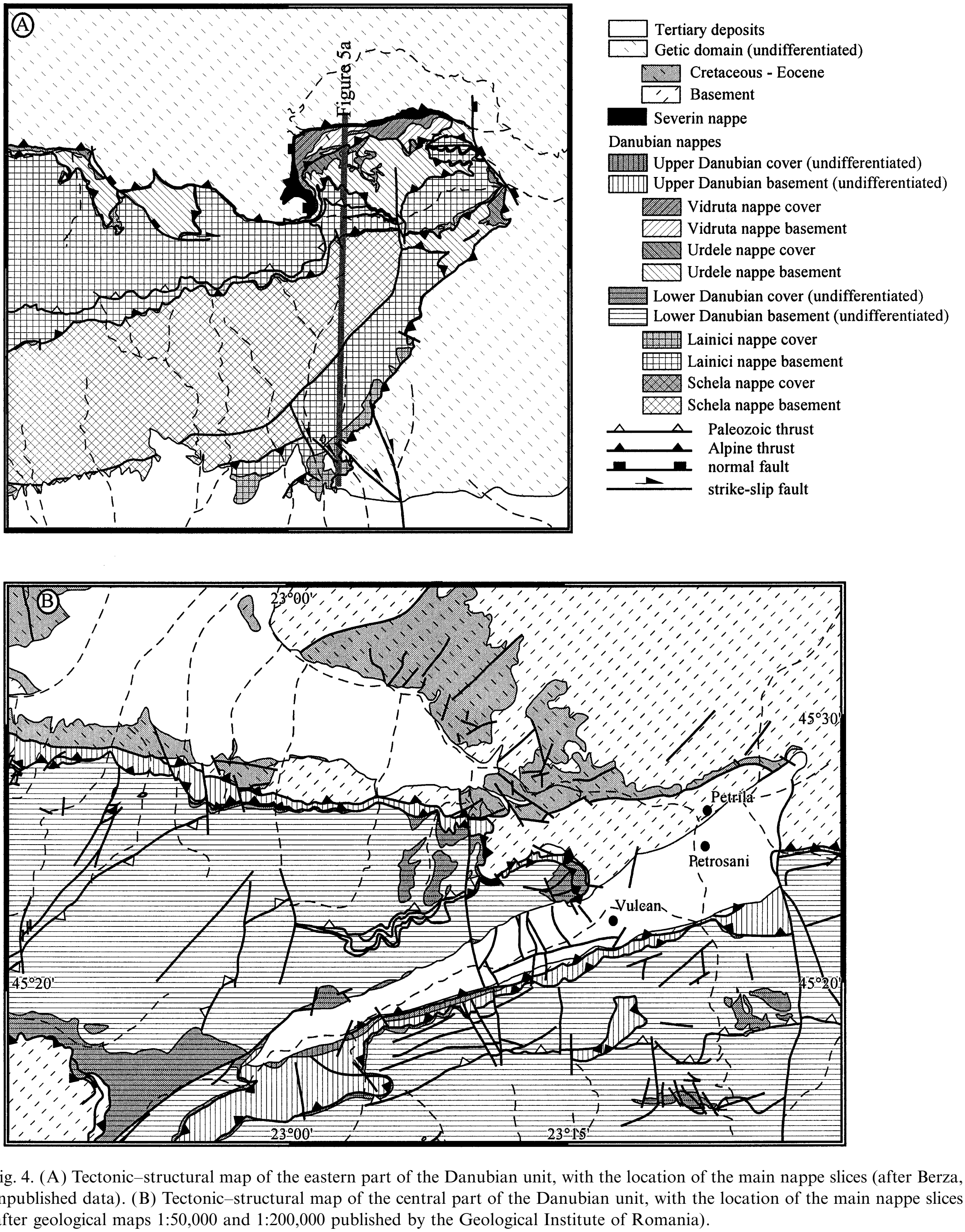

Fig. 4. (A) Tectonic–structural map of the eastern part of the Danubian unit, with the location of the main nappe slices (after Berza, unpublished data). (B) Tectonic–structural map of the central part of the Danubian unit, with the location of the main nappe slices (after geological maps 1:50,000 and 1:200,000 published by the Geological Institute of Romania).

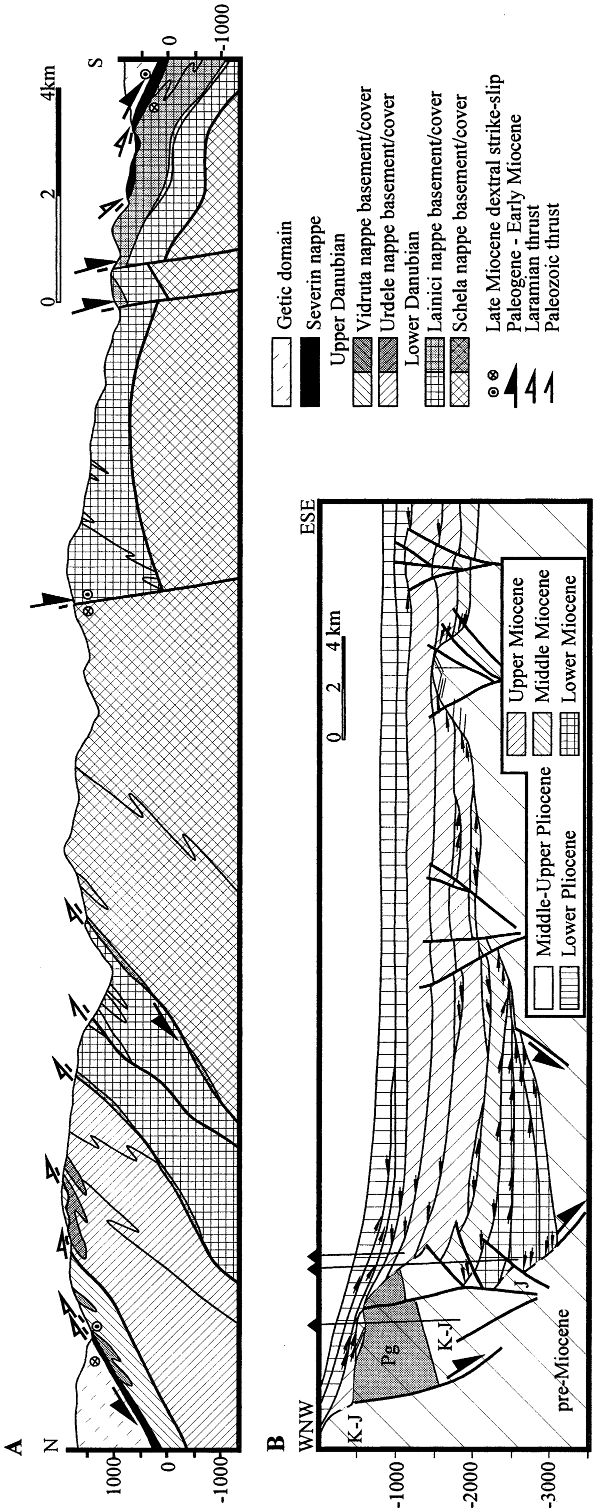

Fig. 5. (A) Regional cross-section across the Danubian unit, modified after Berza (unpublished data) and Schmid et al. (1998). Location in Fig. 3. (B) Interpreted seismic section across the western part of the Getic foredeep. Location in Fig. 1.

strike–slip faults (Fig. 1). Due to petroleum exploration, the sedimentary record and related tectonic events in the foredeep are well dated (e.g. Rabagia and Matenco, 1999). A correlation with less precisely dated Tertiary events in the basement nappes of the South Carpathians will be attempted by the present study.

Paleomagnetic measurements (e.g. Patrascu et al., 1990, 1992, 1994) revealed a clockwise rotation of 50° to 90°, associated with the NE to ENE-ward movement of the Rhodopian fragment and the Tisza–Dacia unit (including the Apuseni mountains) during the Paleogene–Early Miocene (Balla, 1986; Csontos et al., 1992; Ratschbacher et al., 1993; Csontos, 1995; Linzer, 1996; Schmid et al., 1998). Within the South Carpathians this led to the opening of small-scale elongated basins (e.g. the Petrosani, Vidra and Brezoi–Titesti basins, Fig. 1). One would expect this large-scale rotation to significantly affect both foreland structures and structures within the South Carpathians mountains. However, the effects are minor in the sedimentary record, both in the South Carpathians foredeep and in the southern part of the East Carpathians mountains. This suggests strong decoupling between allochthonous units (South and East Carpathians basement nappes) and the Moesian platform.

3. Methods and data

Field data used to reconstruct the tectonic evolution of the Getic and adjacent Danubian nappes were taken from a broad area, mostly adjacent to the Getic detachment. The studied area is bounded to the east by the eastern termination of the Danubian nappes (Voineasa–Lotru valley area) and to the northwest by the Hateg intramontane depression (Fig. 3). Our study mainly focused on outcrops within the Getic nappe, situated in the hanging wall of the Getic detachment and pervasively affected by brittle deformation. The exposed part of the Danubian nappes primarily exhibits mylonite zones, cataclastic zones being largely restricted to the contact zone with the Getic nappe (Schmid et al., 1998). However, a reduced number of brittle structures was also found within the Danubian nappes. For regional correlation, we used information provided by Ratschbacher et al. (1993), Matenco (1997), Schmid et al. (1998), Bojar et al. (1998) and by geological maps 1:200,000 and 1:50,000, published by the Geological Institute of Romania.

Structures such as fault striations, folds, tension joints, fault-related folds (e.g. fault-propagation folds, drag folds) were analysed in 45 locations both in the basement units and in the Mesozoic cover. The combination of fault planes containing slickensides is the most common structure measured. Approximately 1500 outcrop faults with direction and sense of slip were observed in total, each site yielding between 10 and 80 measurements. The slip sense was inferred from kinematic indicators along the fault plane, mostly mineral steps, but also Riedel shears, tectonic tool marks, tension gashes, in-plane conjugate shear fractures, fractures with tension planes, and conjugate fault sets, shear bands in the case of more complex shear zones (Angelier, 1994 and references cited therein; Simpson and Schmid, 1983). The quality of slip sense was classified in the field as certain (54% of fault population), probable (27%), supposed (14%) and unknown (5%). In each site, subsets of fault slip data consistent with different stress directions were separated, on the basis of both the orientation/type of the stress regime and the chronological constraints. The latter were obtained in the field mainly by using criteria such as successive striations on a fault plane, but also from the reactivation of conjugate faults and from cross-cutting relationships. Such criteria were obtained in roughly half of the studied sites. In particular, dextral reactivation of earlier E–W trending Getic sole thrust north of the Danubian unit, or sinistral reactivation of the earlier N–S trending normal faults was observed in many outcrops. The chronology of faulting events due to these reactivations is surprisingly clear in the field, which gives us confidence in the relative timing of these events.

In stations where a sufficient number of faults related to particular stages of deformation was available, generally more than 10 data sets were analysed using the inversion method of Angelier (1984, 1989). The principle of this method is to find the best possible fit between observed fault slip sets and computed shear stresses generated by the stress tensors activating these faults. An interactive programme (Delvaux, 1993) was used for fault data analysis. Inversion of slip direction deduced from kinematic indicators starts with the right dihedron method (Angelier and Mechler, 1977), is optimised firstly with an automatic and secondly with a manual rotational optimisation, in order to fit the best reduced stress tensor to the data set (most commonly minimising the mean slip deviation of the computed shear stress on fault planes from the observed slip sense). This led to the definition of the principal stress axes ($\sigma_1 \geq \sigma_2 \geq \sigma_3$) and the value of the ratio $R=(\sigma_2-\sigma_3)/(\sigma_1-\sigma_3)$ between principal stress magnitudes. A total of 65 reduced stress tensors for all the deformation sets was finally obtained (stereoplots in Figs. 6A, 7A and 8A). This method involves a series of limitations regarding isotropy and tensors, discussed in detail elsewhere (e.g. Angelier, 1984; Etchecopar et al., 1981; Dupin et al., 1993; Pollard et al., 1993). On the basis of the quality of slip sense and of the tensor quality rank (TQR, Delvaux et al., 1997), each tensor was classified as good ($\mathrm{TQR} \geq 1.5$, 7% from the total number of tensors), medium ($0.5 \leq \mathrm{TQR} < 1.5$, 77%) and poor ($0.3 \leq \mathrm{TQR} < 0.5$, 10%) quality (Table 1), while non-reliable tensors ($0.3 < \mathrm{TQR}$, 6%) were rejected.

In places with a low number of measurements, the inversion method was combined with paleostress determinations from two conjugate faults (e.g. Angelier, 1994), minimisation of σ_n on tension joints (Delvaux, 1993) and fault-related fold axis analysis. For the sake of simplicity, only the two conjugate faults were plotted as faults with slip sense (stereoplots in Figs. 6A, 7A and 8A).

The scatter of the fault movements and a second calculation of the kinematic axes were obtained using the Turner (1962) PT axes method (Figs. 6C, 7C and 8C) and the Spang (1972) numeric dynamic analysis method (Figs. 6D, 7D and 8D), by assuming a 30° angle between compressional axes and fault planes.

For the definition of the paleostress field we took into account the nature of the (sub)vertical stress axis and the value of ratio R (Delvaux et al., 1997). Stress fields may vary from extension (σ_1 vertical), with pure extension ($0.25 < R < 0.75$) and transtension ($0.75 < R < 1$), to strike–slip stress fields (σ_2 vertical), with pure strike–slip ($0.25 < R < 0.75$), transtension ($0.75 < R < 1$) and transpression ($0 < R < 0.25$), or to compression (σ_3 vertical), with pure compression ($0.25 < R < 0.75$) and transpression ($0 < R < 0.25$). Radial extension (σ_1 vertical, $0 < R < 0.25$) and radial compression (σ_3 vertical, $0.75 < R < 1$) have been rejected from the calculation, being considered non-conclusive. To constrain the regional stress field, all the stress tensors related to a given deformational stage, as obtained by these methods, were plotted in a single diagram (Figs. 6B, 7B and 8B).

Regional timing constraints were obtained by correlating the observed deformation type, associated with the stress tensors in the South Carpathians, with the age of the similarly deformed sediments (i.e. orientation of fault planes, similar type of slip sense and chronology) in the neighbouring foredeep (Figs. 1 and 2) (see also Matenco et al., 1997a,b; Matenco, 1997). In addition, the extensional deformation revealed by the computed stress tensors was correlated in time with the cooling ages revealed by fission track dating (Sanders, 1998; Schmid et al., 1998; Bojar et al., 1998), which according to Schmid et al. (1998) are associated with a large-scale orogen-parallel extension.

4. Analysis of field data

The analysis of field data and the processing of the fault–slip measurements enabled the description of three major deformation episodes during the Late Cretaceous–Tertiary. We will describe most of the deformation set characteristics, in an old-to-young succession. For each set we will first discuss the general stress parameters and fault data, second the significant associations of structures observed in the outcrop, and finally the map structures that can be correlated with these deformation sets. The described deformation characteristics are plotted on regional-scale maps (Figs. 6, 7 and 8), which allow for further correlations.

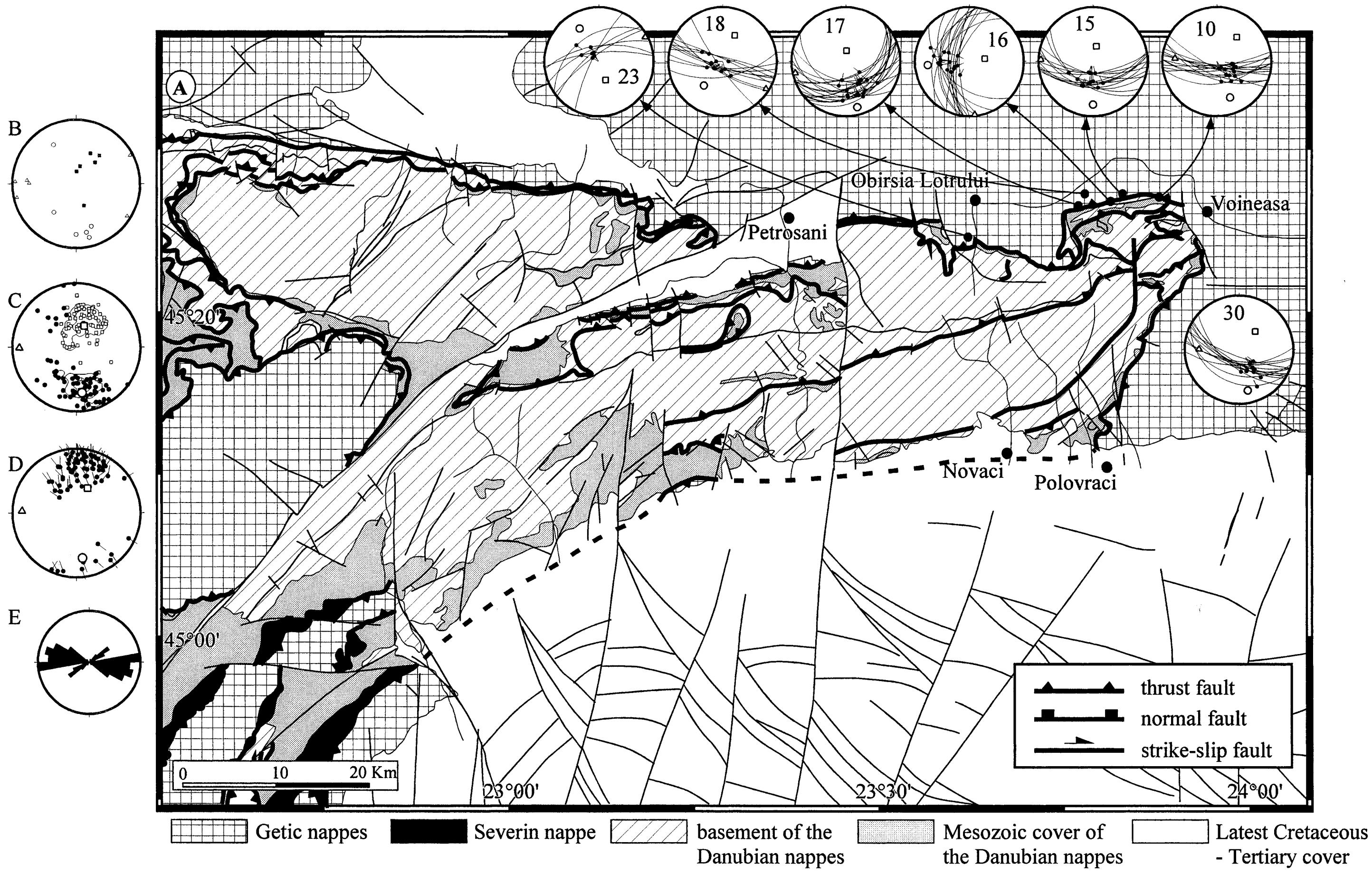

Fig. 6. Brittle deformation structures measured for the Late Cretaceous NNW–SSE compression, $\sigma_1 = 172/15 \pm 20°$, $\pm 20°$ being the aperture of the cone for 95% confidence (Wallbrecher, 1986). (A) Geological–structural map of the studied area with the outcrop measured faults and paleostress tensors (stereoplots) and map-scale active faults during the Late Cretaceous deformation event. Thick black lines are faults with known sense of movement, thick grey lines are faults with possible sense of movement, the dashed line is the supposed prolongation of the Getic detachment below the foredeep cover. Circles are stereoplots of σ_1, triangles are stereoplots of σ_2, rectangles are stereoplots of σ_3. (B) Principal stress axis projections for the direct inversion method for all the paleostress tensors in this deformation event. (C) Projection of the measured compressional and tensional axes for each fault in the measured set, and projections of mean compression, tension and intermediate stress directions, computed using the TURNER method. Contour lines of the compressional and tensional axes are also plotted. (D) Hanging wall movements for the whole faults set (Hoeppener diagram) and principal stress axis computed for the whole faults set using numeric dynamic analysis (NDA) method. (E) Rose diagram with the faults strike for the whole data set.

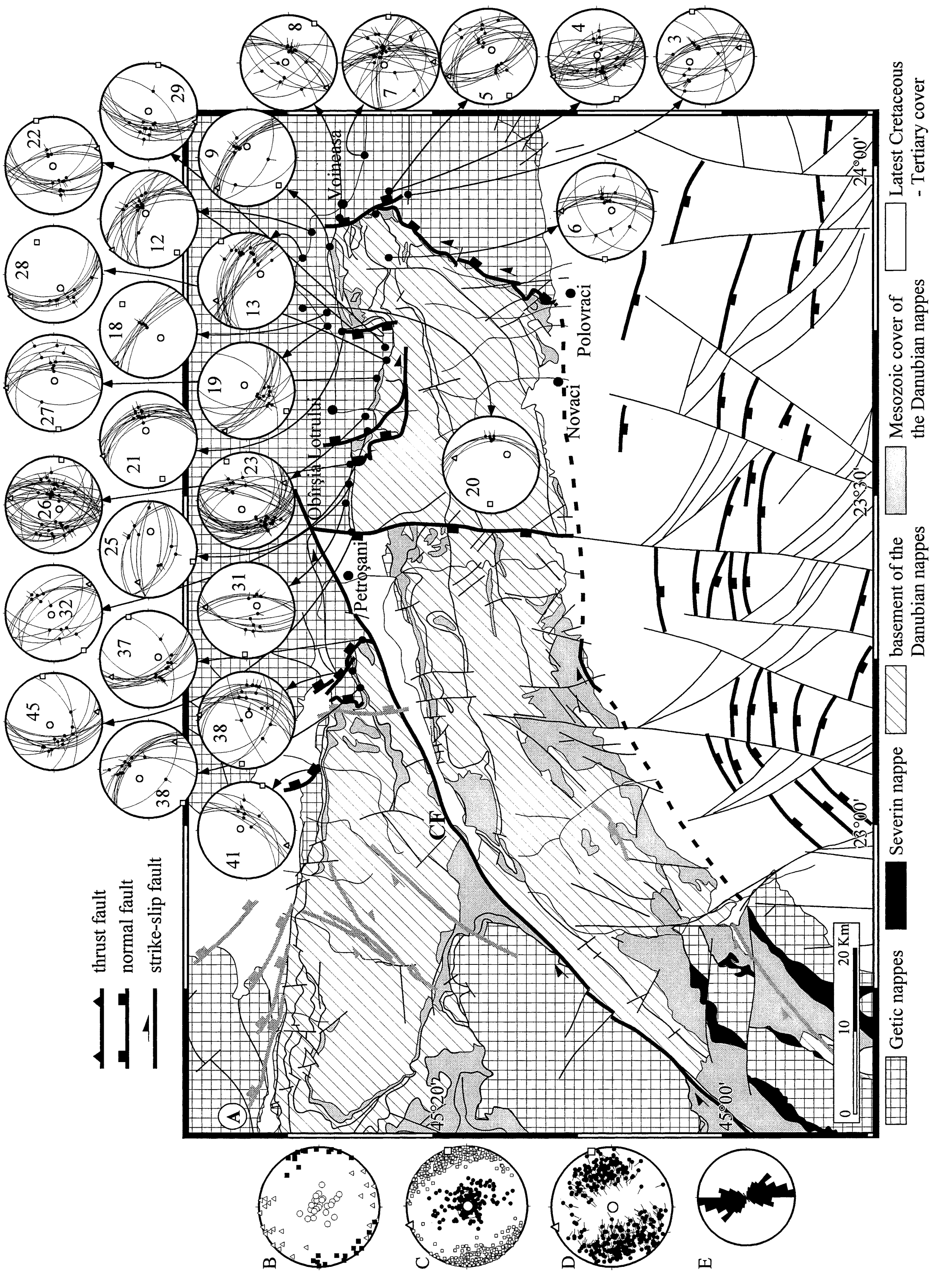

Fig. 7. Brittle deformation structures measured for the Paleogene–Early Miocene WSW–ENE oriented extension, $\sigma_3 = 70/05 \pm 15°$. Conventions as in Fig. 6.

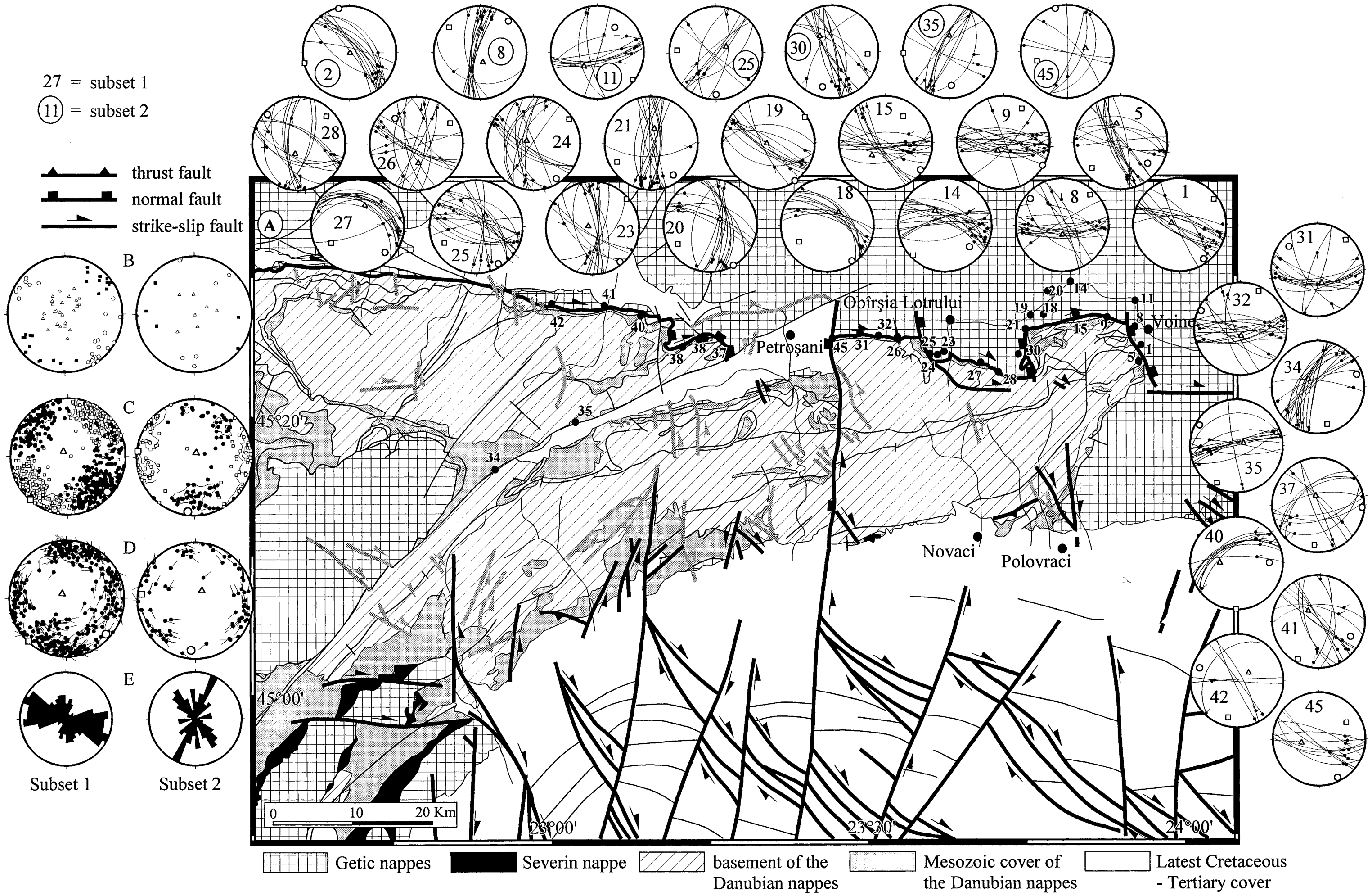

Fig. 8. Brittle deformation structures measured for the Miocene strike–slip. The first subset is characterised by a NW–SE oriented σ_1 (132/8 ± 15°) and a NE–SW trending σ_3 (220/2 ± 15°). The second subset is characterised by a N–S oriented σ_1 (185/06 ± 14°) and W–E σ_3 (275/07 ± 15°). Conventions as in Fig. 6.

Table 1
Location stations and parameters of paleostress reconstruction. Note than only stress tensors obtained with the Angelier (1984, 1989) method are displayed (80% of the total number of tensors computed). n/N represents the number of faults generating a stress tensor versus the total number of faults in the index. σ_1, σ_2, σ_3, azimuth and dip of principal stress axes, σ_1 contraction, σ_2 intermediate, σ_3 extension. R ratio = stress ellipsoid shape factor, $R=(\sigma_2-\sigma_3)/(\sigma_1-\sigma_3)$. α represents the mean slip deviation between the measured kinematic indicator on fault plane and the orientation of the calculated shear stress. TQR = tensor quality rank (Delvaux et al., 1997), TQR $=n(n/N)/\alpha$, where N represents the total number of faults in a data subset, n the number of faults involved in the stress calculation and α the mean slip deviation. D = station measured in the Danubian units, G = station measured in the Getic units

Site	Longitude E	Latitude N	n/N	σ_1	σ_2	σ_3	R	α	TQR	Unit
1S-1	23°55′48″	45°24′19″	13/18	145/11	284/75	53/09	0.69	13.46	B-0.69	G
2S-2	23°57′34″	45°22′52″	14/23	346/02	142/88	256/01	0.83	20.61	C-0.41	D
E-3	23°57′25″	45°22′09″	15/17	341/62	165/28	74/02	0.26	17.65	B-0.74	G
E-4	23°58′21″	45°22′55″	23/27	111/87	335/02	245/02	0.25	13.38	B-1.41	G
E-5	23°56′25″	45°23′13″	16/19	115/77	333/10	242/08	0.57	10.56	B-1.27	D
1S-5	23°56′25″	45°23′13″	17/21	128/28	347/56	228/18	0.27	12.77	B-1.07	D
E-6	23°52′32″	45°22′24″	11/14	170/79	0/11	270/02	0.31	9.38	B-0.92	D
E-7	24°00′02″	45°24′13″	17/21	342/78	178/11	87/03	0.33	12.15	B-1.13	G
E-8	23°56′48″	45°25′31″	13/15	21/84	213/06	123/01	0.52	14.95	B-0.75	G
1S-8	23°56′48″	45°25′31″	16/17	310/12	176/73	43/12	0.39	14.08	B-1.06	G
2S-8	23°56′48″	45°25′31″	12/14	42/10	164/71	309/15	0.42	10.64	B-0.96	G
E-9	23°52′55″	45°26′10″	9/12	88/71	314/14	221/14	0.32	11.00	B-0.61	G/D
1S-9	23°52′55″	45°26′10″	17/21	120/02	216/72	29/18	0.25	14.94	B-0.92	G/D
C-10	23°54′39″	45°25′45″	14/17	160/30	274/24	40/42	0.43	12.66	B-0.91	G
2S-11	23°56′37″	45°26′13″	11/14	35/35	223/55	128/04	0.10	12.98	B-0.66	G
E-12	23°54′00″	45°26′26″	14/18	57/79	320/01	230/11	0.30	14.85	B-0.73	G
E-13	23°52′59″	45°27′45″	20/20	153/63	327/27	58/03	0.64	9.00	A-2.22	G
1S-14	23°50′32″	45°28′37″	18/20	132/30	326/59	226/06	0.41	14.60	B-1.10	G
C-15	23°50′11″	45°25′52″	13/14	180/22	272/05	14/67	0.51	10.80	B-1.11	G
1S-15	23°50′11″	45°25′52″	18/23	128/06	227/57	34/32	0.74	14.45	B-0.97	G
C-16	23°49′18″	45°25′42″	16/16	265/24	174/02	80/66	0.00	10.37	B-1.54	G
C-17	23°46′51″	45°25′31″	19/20	166/15	257/5	5/74	0.45	14.73	B-1.22	G
C-18	23°46′46″	45°26′45″	12/16	218/43	122/06	26/46	0.56	14.08	B-0.63	G
E-18	23°46′46″	45°26′45″	7/8	214/65	313/04	45/25	0.50	3.73	A-1.64	G
1S-18	23°46′46″	45°26′45″	11/13	145/07	43/59	239/30	0.40	19.76	C-0.47	G
E-19	23°46′00″	45°26′45″	12/16	71/80	298/07	207/07	0.55	7.89	B-1.14	G
1S-19	23°46′00″	45°26′45″	13/20	145/01	250/86	55/04	0.50	12.36	B-0.68	G
E-20	23°49′00″	45°27′52″	6/7	147/57	11/25	271/20	0.45	14.24	C-0.48	G
1S-20	23°49′00″	45°27′52″	16/16	150/01	57/69	240/21	0.19	16.17	B-0.98	G
E-21	23°45′18″	45°25′27″	13/13	73/74	340/01	250/15	0.70	9.41	B-1.38	G/D
1S-21	23°45′18″	45°25′27″	16/21	145/18	14/64	241/18	0.54	9.70	B-1.25	G/D
DE-22	23°45′07″	45°24′36″	13/13	323/88	159/02	69/01	0.75	15.04	B-0.86	G/D
C-23	23°36′49″	45°25′21″	7/8	330/30	62/04	159/60	0.36	6.96	B-0.88	G
E-23	23°36′49″	45°25′21″	30/36	297/73	155/13	63/10	0.67	14.68	A-1.70	G
1S-23	23°36′49″	45°25′21″	15/20	141/07	292/82	50/04	0.38	15.20	B-0.74	G
1S-24	23°36′21″	45°24′49″	15/24	147/11	292/77	56/08	0.35	16.19	B-0.57	G
E-25	23°34′51″	45°24′45″	9/9	98/59	287/30	195/05	0.83	14.43	B-0.62	D
1S-25	23°34′51″	45°24′45″	19/25	149/08	40/64	243/24	0.57	15.63	B-0.92	D
2S-25	23°34′51″	45°24′45″	10/13	180/11	59/69	274/18	0.80	17.25	C-0.44	D
E-26	23°32′46″	45°24′44″	35/43	218/78	9/11	100/06	0.40	12.91	A-2.20	G/D
1S-26	23°32′46″	45°24′44″	16/25	320/30	173/55	59/16	0.38	7.98	B-1.28	G/D
E-27	23°40′02″	45°23′15″	10/14	110/86	354/02	264/04	0.64	16.77	C-0.42	G/D
1S-27	23°40′02″	45°23′15″	11/16	134/19	20/51	237/33	0.50	10.43	B-0.72	G/D
E-28	23°41′00″	45°23′03″	9/12	243/64	333/00	63/26	0.53	14.23	C-0.47	G
1S-28	23°41′00″	45°23′03″	15/22	313/08	199/71	46/17	0.50	18.04	B-0.56	G
E-29	23°42′41″	45°23′08″	11/14	357/89	193/01	102/1	0.78	11.63	B-0.74	G
C-30	23°44′51″	45°23′21″	13/13	168/24	271/27	42/53	0.47	5.16	A-2.51	G

Table 1 (*continued*)

Site	Longitude E	Latitude N	n/N	σ_1	σ_2	σ_3	R	α	TQR	Unit
2S-30	23°44′51″	45°23′21″	14/17	195/23	323/55	94/24	0.28	10.10	B-1.14	G
E-31	23°28′18″	45°25′10″	10/11	156/70	5/18	272/09	0.44	9.42	B-0.96	G
1S-31	23°28′18″	45°25′10″	14/17	310/21	161/66	44/11	0.57	12.70	B-0.90	G
E-32	23°29′14″	45°25′03″	11/11	322/85	141/05	231/00	0.25	9.29	B-1.18	G
1S-32	23°29′14″	45°25′03″	18/21	295/07	173/77	26/11	0.50	10.54	B-1.46	G
1S-34	22′54′35″	45°16′27″	17/20	72/12	310/68	166/18	0.51	15.33	B-0.94	D
1S-35	23°01′32″	45°19′21″	14/15	300/09	68/76	208/11	0.61	21.08	B-0.61	D
2S-35	23°01′32″	45°19′21″	11/11	177/28	358/62	268/01	0.52	11.64	B-0.94	D
E-37	23°16′14″	45°24′05″	11/11	168/73	334/17	65/04	0.28	15.35	B-0.71	G
1S-37	23°16′14″	45°24′05″	12/14	93/05	347/73	185/16	0.49	10.65	B-0.96	G
E-38	23°12′21″	45°24′41″	15/19	113/79	7/03	276/11	0.29	15.80	B-0.74	D
E-38	23°12′21″	45°24′41″	11/12	314/68	134/22	224/00	0.41	14.80	B-0.68	D
1S-40	23°07′48″	45°26′37″	9/9	90/30	272/60	181/00	0.40	10.85	B-0.82	D
E-41	23°04′18″	45°27′10″	7/10	15/79	200/11	110/01	0.28	14.57	C-0.33	G
1S-41	23°04′18″	45°27′10″	12/16	115/24	316/64	209/08	0.58	15.85	B-0.56	G
1S-42	23°01′18″	45°26′58″	6/10	289/16	57/65	194/19	0.68	4.67	B-0.77	G
E-45	23°26′36″	45°25′10″	12/12	320/81	167/08	76/04	0.40	11.01	B-1.08	G
1S-45	23°26′36″	45°25′10″	10/12	154/09	259/58	59/31	0.75	13.58	B-0.61	G
2S-45	23°26′36″	45°25′10″	7/10	345/04	81/57	252/32	0.42	14.14	C-0.34	G

4.1. NNW–SSE contraction

The first data set (Fig. 6) is characterised by a NNW–SSE compressional stress regime (Fig. 6B). The orientations of the calculated tensors display a certain degree of dispersion, one tensor (C-16) having a roughly E–W compression direction (Fig. 6A), whereas the TQR values show medium to good quality tensors (Table 1). R values show pure compressional to transpressional character (Table 1). In the field, deformation linked to this data set is characterised by a small number of thrust faults with SSE vergence and primarily by backthrusts with NNW vergence (stereoplots in Fig. 6A and D). At the outcrop scale, WSW–ENE trending faults (Fig. 6E) are mostly associated with cataclastic zones, often with shear bands and Riedel shears criteria of slip. All the measured faults related to this data set are located in the hanging wall of the Getic detachment. On the regional and local scale, the thrusts related to this data set clearly predate the normal and strike–slip faults linked with the second and, respectively, third data set.

4.2. WSW–ENE extension

The second data set (Fig. 7) is characterised by a WSW–ENE extensional stress regime (Fig. 7B). A very good concentration of the obtained tensors is observed (Fig. 7C). The slip deviation factor, which 'compares' the observed faults striae with the shear plane determined by the calculated tensor, is low. This reflects deformation characterised by well-oriented fault plane populations. For a majority of the stations the R ratio indicates pure extension, two stations (E-25, E-29, Table 1, location in Fig. 7A) being transtensive. The computed tensors are of medium to good quality (TQR, Table 1). A large number of normal faults are observed in outcrop scale, associated with this WSW–ENE extensional stage. Top-to-ENE normal faults dominate, but associated top-to-WSW normal faults occur (Fig. 7D). Normal faults have a NNW–SSE strike in the easternmost Voineasa–Obarsia Lotrului areas, whereas in the western areas the dominant trend is N–S (stereoplots in Fig. 7A and E). This data set often reveals structures formed at the ductile–brittle transition, stria on the same outcrop often being associated with both purely cataclastic zones and ductile shear bands. Most of the stations are located within the Getic nappe and near the Getic detachment, but widespread normal faulting with the same characteristics is also observed away from the detachment and within the Getic units (within the studied area and further to the east, i.e. in the Olt valley area, see also Matenco et al., 1997a,b). A limited number of brittle normal faults were also measured within the Danubian nappe system. Here, brittle faults often overprint mylonites, shear bands grading into Riedel shears of identical orientation and sense of movement.

4.3. Strike–slip regime

The third data set comprises the largest number of fault data and was recognised over the entire area, being characterised by strike–slip deformation (Fig. 8). Two subsets have been defined on the basis of different orientations of σ_1 and σ_3 axis, both having medium quality tensors (TQR, Table 1). The relative timing relationships between the two subsets, as occasionally seen in the field, indicate reactivation of fault planes belonging to the first subset (subset 1, Fig. 8) by the second subset (subset 2, Fig. 8).

The first subset (subset 1, Fig. 8) is characterised by a NW–SE compression and a NE–SW tension (Fig. 8B). Deformation is characterised by a low slip deviation factor (Table 1), a well marked trend of the strike–slip faults being observed in the field (Fig. 8C). The most common large-scale structures developed during this stage are sets of conjugate strike–slip faults. E–W to WNW–ESE oriented dextral faults predominate over N–S to NNW–SSE trending sinistral faults (Fig. 8D and E and stereoplots in Fig. 8A). Most of the dextral strike–slip faults were measured at or near the Getic detachment. Where this contact turns to a more N–S oriented trend, sinistral faults dominate.

The second subset (subset 2, Fig. 8) is characterised by a strike–slip regime with N–S compression and W–E tension (Fig. 8B). The concentration of the obtained tensors is good (Fig. 8C). The slip deviation from the theoretical general tensor is low, thus reflecting deformation along fault planes with fairly constant strike along the belt. Most *R* ratios have a pure strike–slip character. Transtensional *R* values are found along or near the Getic detachment (Table 1, locations in Fig. 8A). Usually, NW–SE striking sinistral transcurrent faults dominate, but associated NNE–SSW trending sinistral faults are also observed in the field (Fig. 8D and E and stereoplots in Fig. 8A). The faults associated with this data set show a random spatial distribution recognised in the entire studied area, without clear zonal preferences.

A direct discrimination of the two subsets is often difficult to make in the field. In both cases deformation is purely brittle, indicating that it took place in a shallower structural level than the previous extension, which it clearly post-dates, as observed along the reactivated fault planes. The separation into two subsets, largely based on the slightly different stress axes and little superposition evidence, is strongly supported by the two different sets of strike–slip faults: a dextral set pre-dates a sinistral one, as observed in the foredeep in map scale (see below and Fig. 2).

5. Tectonic evolution

Our analysis of brittle deformation can be correlated with the kinematic analysis of ductile deformations and fission track timing (Schmid et al., 1998). Together with the structures observed in the adjacent foredeep (e.g. Matenco, 1997; Rabagia and Matenco, 1999) this allows for the definition of three major deformation episodes in the central–southern part of the South Carpathians during Late Cretaceous to Tertiary times.

5.1. Late Cretaceous (Laramian) contraction

The first data set may be correlated with the major emplacement of the Getic nappe and the Severin nappe at its base over the Danubian nappes during Late Cretaceous times (so-called Laramian phase) (Fig. 2). Our analysis of brittle deformation features within the Getic nappe, indicating a compressional stress regime with NNW–SSE oriented σ_1, is in agreement with NNW-SSE trending mylonitic stretching lineations in deeper tectonic levels, within the Danubian nappe stack (Schmid et al., 1998). These authors ascribed this older generation of stretching lineations to top SSE nappe stacking, in agreement with Seghedi and Berza (1994). Nappe stacking (Fig. 5A) is related to brittle deformation within the Getic nappe, while ductile deformation under lower greenschist facies conditions prevailed within the Danubian nappes. The main associated structures formed during this episode are WSW–ENE trending thrusts (Figs. 5A and 6A) with top-SSE sense of shear (Schmid et al., 1998). However, associated top-NNW backthrusts can also be observed in the field (see also Berza et al., 1994).

The timing of this deformation episode is poorly constrained. It post-dates Danubian turbidites of Turonian to Senonian age and some of these thrusts are covered by the Latest Cretaceous (Maastrichtian) deposits in the Hateg basin and Oligocene deposits of the Petrosani basin. A Late Cretaceous age (76–72 Ma) is indicated by Rb–Sr muscovite ages from the Danubian nappes, interpreted as formation ages (Ratschbacher et al., 1993), while other radiometric ages from the Danubian units span the 120–70 Ma time interval. Late Cretaceous deformation is penetrative and can reach lower geenschist facies conditions (Ciulavu and Ferreiro-Mählmann, 1999).

5.2. Paleogene–Early Miocene extension

The second data set can be correlated with the large-scale orogen-parallel extension leading to core complex formation and exhumation of the Danubian units below the Getic detachment (Schmid et al., 1998) (Figs. 2 and 9A). The ENE direction of σ_1 (70°) derived in this study is similar to the mean azimuth of mylonitic lineations (64°) in both the Danubian units and the Getic detachment (Schmid et al., 1998). Ductile mylonitisation is restricted to the footwall of the Getic detachment, where exhumation of the eastern Danubian units locally induced a modest, late overprinting by brittle structures. Exclusively brittle manifestations of this deformation episode are found in the Getic nappe. The fission track data (Schmid et al., 1998) indicate that exhumation of the greenschist facies eastern Danubian units related to normal faulting underneath the east dipping Getic detachment started in the Late Eocene and terminated during the Early Oligocene. In the Getic nappe brittle deformation prevailed during the entire period of extension, while the onset of brittle overprint in the Danubian nappes may be estimated to closely coincide with the zircon fission track ages found in this unit (40–46 Ma in the western, and 30–31 Ma in the eastern part of the Parang mountains).

North of the Danubian window the mylonites related to the Getic detachment are north dipping and WNW–ESE striking due to the updoming of the Danubian units, interpreted to be the result of contemporaneous E–W extension and moderate N–S compression (Schmid et al., 1998). NNW–SSE to N–S trending brittle normal faults dissect and/or overprint the mylonites related to the Getic detachment on the map scale (Fig. 7A). Normal faulting locally caused a N–S to NNW–SSE trend of the contact between Getic and Danubian units. E to ENE-ward dipping faults, synthetic to the Getic detachment predominate, but antithetic W to WSW-ward dipping faults were also measured. Some of these faults displace earlier formed mylonites related to the Getic detachment, the mylonites extension direction being unchanged with respect to the brittle extension. We interpret the latter to have formed during the late stages of core complex formation, when earlier formed mylonites also become affected by brittle faulting due to ongoing exhumation of the Danubian units.

The most important brittle structure, a large-scale ENE dipping normal fault, is found at the eastern termination of the Danubian window, in the Voineasa area (Fig. 7A). Other major N–S trending normal faults are either W-ward dipping, like east of Obarsia Lotrului and at the eastern termination of the Petrosani basin, or E-ward dipping, like S and SE of the Hateg basin and west of Obarsia Lotrului. Due to large-scale uplift and exhumation of the Danubian nappes below the Getic detachment, the original NNW dip of the frontal part of the Cretaceous Getic sole thrust has been rotated and is presently observed to dip to the SSE (Fig. 9C).

Other large-scale features linked to this deformation episode are NE–SW to ENE–WSW trending dextral faults, linked to the activation of the coeval clockwise rotation and dextral shearing around the Moesian corner (e.g. Ratschbacher et al., 1993; Schmid et al., 1998). The most important is the Cerna fault, which offsets the northern margin of the Danubian nappes by some 35 km

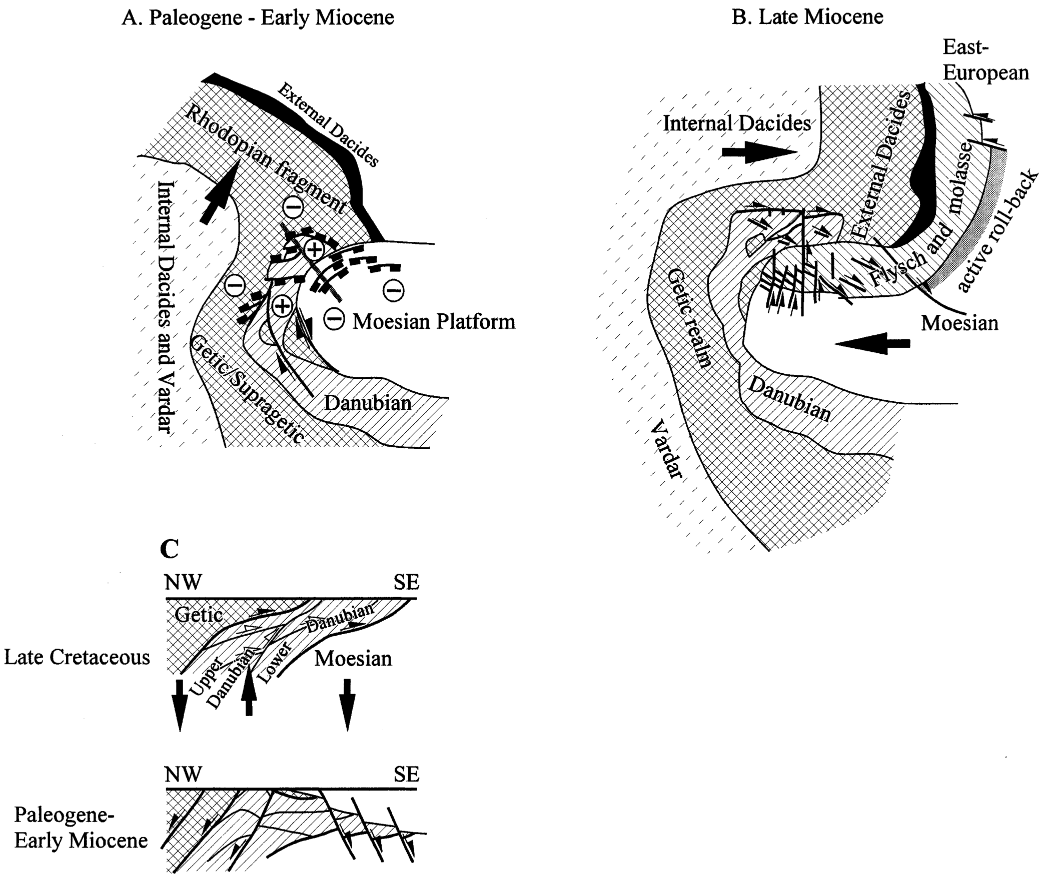

Fig. 9. Tectonic model for the Tertiary deformations of the central part of the South Carpathians. (A) Paleogene–Early Miocene extension. + represents areas uplifted in respect to − adjacent areas. (B) Late Miocene strike–slip. (C) Model for the Danubian exhumation, uplift and Getic sole thrust rotation from NNW dipping to SSE dipping.

(Berza et al., 1983; Berza and Draganescu, 1988). Since this fault is Oligocene in age (Ratschbacher et al., 1993) and offsets the Getic detachment, it shortly post-dates the orogen-parallel extension.

Large-scale extension during this episode is also observed in the adjacent southern foredeep of the South Carpathians (e.g. Fig. 5B). The age of normal faulting is documented for the Lower Miocene, possibly starting during the Paleogene (Matenco et al., 1997a,b; Rabagia and Matenco, 1999), constrained by Paleogene deposits in the footwall of most normal faults, pre-dating well-dated Middle Burdigalian deposits in the hanging wall. Subvertical normal faults formed here within an E–W oriented corridor of dextral transtension, related to NE-ward movement of the South Carpathians with respect to Moesia, and hence compatible with a roughly NE oriented direction of the least principal stress (Fig. 9A). The presently observed ENE–WSW Paleogene extension directions observed near the Getic detachment may have been subsequently rotated due to Oligocene clockwise rotation around the Moesian corner, related to the activity along the Cerna and other curved dextral faults (Schmid et al., 1998). The Lower Miocene corridor within the Getic Depression indicates a foreland migration of the transtensional deformation after the Oligocene (Fig. 2).

In summary, the overall extension within the South Carpathians and in the foredeep seems to develop in two main stages during the Paleogene to Early Miocene episode (Fig. 9A). The first stage (Eocene–Early Oligocene) pre-dates rotation along the Oligocene Cerna and Timok faults system and is poorly documented in the foredeep (e.g. Paleogene depocenter in the WNW part of Fig. 5B) but coeval with orogen-parallel extension in the Getic/Danubian nappes, causing their exhumation. The second Early Miocene extensional stage post-dates major Oligocene clockwise rotation along curved dextral strike–slip faults and is still associated with a NE–SW oriented direction of minimum principal stress in the South Carpathians foredeep.

5.3. Late Miocene strike–slip movements

The third data set relates to Late Miocene dextral translation taking place within an E–W oriented corridor crossing the South Carpathians mountains and dextral transpressive shearing within the southern foredeep (Fig. 8A). This deformation leads to further E-ward movement of the South Carpathians hinterland with respect to the Moesian platform (Fig. 9B). Due to the low seismic resolution in the foredeep at great depth, it is not clear how much of the dextral displacement was accomplished already during the previous Oligocene transtensive dextral event.

In the Getic Depression, deformation took place in two episodes (Matenco, 1997; Rabagia and Matenco, 1999). A first Late Miocene episode (13–11 Ma, Early to Middle Sarmatian, sensu Eastern Paratethys) led to WNW–ESE to NW–SE dextral faulting which slightly pre-dates a second Latest Miocene–Early Pliocene strike–slip episode (11–9 Ma, Late Sarmatian–Meotian), characterised by N–S to NNE–SSW trending sinistral faults and transpressive reactivation of the earlier dextral systems (Figs. 1, 3, 5B and 8A).

In the South Carpathians mountains, poor timing prevents precise dating of the strike–slip movements. On the map scale, the same two major sets of faults as observed in the foredeep can be recognised.

The main faults are dextral and oriented E–W to NE–SW (Fig. 8A). E–W dextral indicators are found in almost all the stations located within the Getic nappe and near the Getic detachment. This suggests an E-ward movement of the Getic nappes with respect to the Danubian units, reactivating the earlier formed Getic detachment. A major EW striking dextral fault is observed south of Voineasa, representing the western prolongation of a Miocene dextral fault bounding the Brezoi–Titesti basin to the south (see also Matenco et al., 1997a,b). Its dextral strike–slip movement is transferred westward by the reactivation of an earlier normal fault, situated at the western end of the Danubian window. A similar dextral displacement transfer is given by a normal fault mapped immediately west of Obarsia Lotrului (Fig. 8A). Smaller scale dextral faults are observed further west, overprinting the Getic detachment. These faults have an E–W trend in the northern parts and are NW–SE oriented towards the south.

The N–S to NNE–SSW trending sinistral fault system is also observed within the South Carpathians mountains (Fig. 8A). In outcrop and map scale it truncates the dextral system, and is therefore younger. The most important sinistral structure is a N–S fault bounding the Petrosani basin to the east, which reactivates an older Paleogene normal fault. Interestingly, this major fault can be followed into the foredeep, where an offset of 5 km is observed, the total length exceeding 80 km (Fig. 1). Smaller scale sinistral faults are observed between the Danubian thrust sheets or truncating the Getic detachment (Fig. 8A).

On a regional scale, dextral deformation taking place between the Getic and the Danubian units along the E–W oriented segments of the Getic detachment was connected through the E–W extensional reactivation of the N–S trending pre-existent normal faults, which acted as transfer zones. Dextral deformation was transferred further to the east, out of the studied area and towards the Intramoesian fault (Matenco, 1997) (Fig. 1).

6. Conclusions

The Late Cretaceous–Tertiary evolution of the central South Carpathians can be described in terms of three deformation episodes: (1) Late Cretaceous contraction; (2) Paleogene to Early Miocene extension, combined with dextral transtension and rotation along curved dextral strike slip faults (Cerna and Timok faults); and (3) Late Miocene predominantly dextral strike–slip movements, pure right-lateral to transtensive in the South Carpathians and transpressive in the South Carpathians foredeep.

NNW–SSE oriented contraction during the Late Cretaceous was responsible for the final emplacement of the Getic and Severin nappes over the Danubian nappe system, pre-dating the thick post-tectonic Late Cretaceous–Early Paleogene sedimentation in the foredeep and some intramontane (e.g. Hateg) basins. Mostly E–W to ENE–WSW trending thrusts and subordinate backthrusts led to final nappe stacking and duplex formation in the Danubian units (Berza et al., 1994). This period may be correlated with the Late Cretaceous deformation phase affecting the entire Romanian Carpathians (Sandulescu, 1984, 1988).

During the Paleogene–Early Miocene, large-scale orogen-parallel extension took place in the South Carpathians and led to rapid uplift and exhumation of the Danubian basement in the footwall of the Getic detachment. Three steps can be distinguished in the general Paleogene–Early Miocene evolution. During the Eocene–Early Oligocene the major exhumation and uplift of the Danubian units took place along the Getic detachment, reactivating the Late Cretaceous Getic sole thrust. During the Middle–Late Oligocene, the NE to E-ward clockwise rotation of the Inner Carpathians around Moesia (see also Ratschbacher et al., 1993; Schmid et al., 1998) led to activation of the dextral curved trace Cerna and Timok faults system, reorienting originally WSW–ENE trending Getic detachment north of the Danubian window into the present NNW–SSE trend. During the Lower Miocene, extension migrated towards the South Carpathians foredeep, the continued NE-ward movement of the inner Carpathians leads to the opening of a large-scale dextral pull-apart basin. The main normal faults controlling the opening of the basin formed parallel to the regional WSW–ENE to W–E dextral movement, as observed recently in other case studies (e.g. Ben-Avraham and Zoback, 1992).

Large scale E-ward translation took place along dextral strike–slip faults during the Late Miocene, the E-ward movement of the inner Carpathians allowed the E–W directed major contraction in the East Carpathians. A first dextral corridor developed in the southern foredeep zone and a second translation zone developed along the Getic detachment, north of the Danubian units.

Plate tectonic models assume that the Carpathians formed as a consequence of the NE to E-ward translation of several continental (Rhodopian) blocks and final collision with the East-European/Scythian/Moesian platforms system (Sandulescu, 1984; Csontos, 1995; Matenco, 1997 and references cited therein). According to the traditional interpretation, the Eocene–Oligocene extension in the East Carpathians was followed by three Miocene contractional events, of which only the last one would affect the South Carpathians (e.g. Sandulescu, 1984, 1988). More recent models (Csontos et al., 1992; Ratschbacher et al., 1993; Csontos, 1995; Linzer, 1996; Zweigel, 1997; Linzer et al., 1998; Schmid et al., 1998; Zweigel et al., 1998) generally assume more continuous deformation. A general E-ward translation of the Carpathians system was accommodated first through top-ENE extensional deformation during the Paleogene, and second through dextral translation between the Moesian Platform and more internal units. This translation is considered to be triggered by the E-ward directed roll-back of the distal part of the autochthonous platforms in the frontal part of the East Carpathians (Royden, 1988).

Our reconstruction of the Tertiary deformations of the Getic/Danubian system in the central part of the South Carpathians is compatible with these models. These findings support the definition of regional extensional deformation taking place in the basement units of the South Carpathians during the Early Tertiary. The foreland migration character of normal faulting and the large-scale dextral transfer taking place at the basement units contact supports the regional Tertiary eastward movement of the South Carpathians basement units with respect to the Moesian platform.

Acknowledgements

The research carried out in this paper was possible due to Swiss National Science Foundation support (Grant 7RUPJ048623). The research of LM was additionally supported by the Romanian Academy of Sciences and the Romanian Ministry of Research and Technology (Grants 4046GR and 1874). T. Berza, V. Diaconescu, C. Dinu, V. Mocanu, N. Froitzheim are thanked for sharing experience in the area, scientific and logistic support and for the local geological background and for nice moments spent together in the field. We gratefully acknowledge the editorial comments of J.P. Burg, and the reviews of L. Ratschbacher and F. Neubauer, which have substantially improved this paper. The PANCARDI project of EUROPROBE, financed by European Science Foundation was essential in providing links for international cooperation.

References

Angelier, J., 1984. Tectonic analysis of fault slip data sets. J. Geophys. Res. 89, 5835–5848.

Angelier, J., 1989. From orientation to magnitudes in paleostress determination using fault slip data. J. Struct. Geol. 11, 37–50.

Angelier, J., 1994. Fault slip analysis and paleostress reconstruction. In: Hancock, P.L. (Ed.), Continental Deformation. Pergamon, New York, pp. 53–100.

Angelier, J., Mechler, P., 1977. Sur une methode graphique de recherche des contraintes principales egalement utilisable en tectonique et en seismologie: La methode des diedres droits. Bull. Soc. Geol. Fr. 7, XIX6, 1309–1318.

Balintoni, I., Berza, T., Hann, H.P., Iancu, V., Kräutner, H.G., Udubasa, G., 1989. Precambrian metamorphism in the South Carpathians in: Guide to Excursions, Problem commision IX, 23–45.

Balla, Z., 1986. Paleotectonic reconstruction of the central Alpine–Mediteranean belt for the Neogene. Tectonophysics 127, 213–243.

Ben-Avraham, Z., Zoback, M.D., 1992. Transform-normal extension and asymmetric basins: An alternative to pull-apart models. Geology 20, 423–460.

Berza, T., Draganescu, A., 1988. The Cerna–Jiu fault system (South Carpathians, Romania), a major Tertiary transcurrent lineament. D.S. Inst. Geol. Geofiz. 72/73, 43–57.

Berza, T., Iancu, V., 1994. Variscan events in the basement of the Danubian nappes (South Carpathians). In: Berza, T. (Ed.), Geological evolution of the Alpine–Carpathian–Pannonian system, ALCAPA II, field guidebook, Rom. J. Tect. Reg. Geol., 93–104.

Berza, T., Kräutner, H.G., Dimitrescu, R., 1983. Nappe structure of the Danubian window of the central South Carpathians. An. Inst. Geol. Geofiz. 60, 31–34.

Berza, T., Balintoni, I., Iancu, V., Seghedi, A., Hann, H.P., 1994. South CarpathiansGeological evolution of the Alpine–Carpathian–Pannonian system, ALCAPA II, field guidebook, Berza, T. (Ed.), Rom. J. Tect. Reg. Geol., 37–49.

Bojar, A.V., Neubauer, F., Fritz, H., 1998. Jurassic to Cenozoic thermal evolution of the southwestern South Carpathians: evidence from fission-track thermochronology. Tectonophysics 297, 1–4, 229–249.

Burchfiel, B.C., 1976. Geology of Romania, Special Paper 158. Geological Society of America. 82 pp.

Ciulavu, M., Ferreiro-Mählmann, R., 1999. The alpine metamorphic pattern in the Danubian window, South Carpathians (Romania). Abstract EUG 10.

Codarcea, A., 1940. Vues nouvelles sur la tectonique du Banat et du Plateau du Mehedinti. An. Inst. Geol. Rom. XX, 1–74.

Csontos, L., 1995. Tertiary tectonic evolution of the Intra-Carpathian area: a review. Acta Vulcanol. 7, 1–13.

Csontos, L., Nagymarosy, A., Horvath, F., Kovac, M., 1992. Tertiary evolution of the intra-Carpathian area: a model. Tectonophysics 208, 1–3.

Dallmeyer, R.D., Neubauer, F., Fritz, H., Mocanu, V., 1998. Variscan vs. Alpine tectonothermal evolution of the Southern Carpathians orogen: constraints from 40Ar/39Ar ages. Tectonophysics 290, 111–135.

Delvaux, D., 1993. The TENSOR program for paleostress reconstruction: examples from the east African and the Baikal region, Central Asia. Terra Nova 5 Abstr. Suppl., 216

Delvaux, D., Moeys, R., Stapel, G., Petit, C., Levi, K., Miroshnichenko, A., Ruzhich, V., San'kov, V., 1997. Paleostress reconstruction and geodynamics of the Baykal region. Tectonophysics 282, 1–4, 1–38.

Dicea, O., 1995. The structure and hydrocarbon geology of the Romanian East Carpathians border from seismic data. Petrol. Geosci. 1, 135–143.

Dupin, J.M., Sassi, W., Angelier, J., 1993. Homogenous stress hypothesis and actual fault slip: a distinct element analysis. J. Struct. Geol. 15 (8), 1033–1043.

Etchecopar, A., Vasseur, G., Daignieres, M., 1981. An inverse problem in microtectonics for the determination of stress tensors from fault striation analysis. J. Struct. Geol. 3 (1), 51–65.

Iancu, V., Maruntiu, M., 1994. Pre-Alpine litho-tectonic units and related shear zones in the basement of Getic–Supragetic nappes (South Carpathians). In: Berza, T. (Ed.), Geological evolution of the Alpine–Carpathian–Pannonian system, ALCAPA II, field guidebook, Rom. J. Tect. Reg. Geol., 87–92.

Liegois, J.P., Berza, T., Tatu, M., Duchesne, J.C., 1997. The Neoproterozoic Pan-African basement from the Alpine Lower Danubian nappe system (South Carpathians, Romania). Precambrian Res. 80, 281–301.

Linzer, H.G., 1996. Kinematics of retreating subduction along the Carpathian arc, Romania. Geology 24, 167–170.

Linzer, H.-G., Frisch, W., Zweigel, P., Girbacea, R., Hann, H.-P., Moser, F., 1998. Kinematic evolution of the Romanian Carpathains. Tectonophysics 297, 1–4, 133–156.

Matenco, L., 1997. Tectonic evolution of the Outer Romanian

Carpathians: Constraints from kinematic analysis and flexural modelling. Ph.D. Thesis, Vrije Universiteit, Faculty of Earth Sciences, Amsterdam, 160 pp.

Matenco, L., Bertotti, G., Dinu, C., Cloetingh, S., 1997a. Tertiary tectonic evolution of the external South Carpathians and the adjacent Moesian platform (Romania). Tectonics 16 (6), 896–911.

Matenco, L., Zoetemeijer, R., Cloetingh, S., Dinu, C., 1997b. Lateral variations in mechanical properties of the Romanian external Carpathians: inferences of flexure and gravity modelling. Tectonophysics 282, 147–166.

Murgoci, G.M., 1912. The geological synthesis of the South Carpathians. C.R. XI Cong. Geol. Int., 871–881.

Patrascu, S., Bleahu, M., Panaiotu, C., 1990. Tectonic implications of paleomagnetic research into Upper Createaceous magmatic rocks in the Apuseni Mountains, Romania. Tectonophysics 180, 309–322.

Patrascu, S., Bleahu, M., Panaiotu, C., Panaiotu, C.E., 1992. The paleomagnetism of the Upper Cretaceous magmatic rocks in the Banat area of South Carpathians: tectonic implications. Tectonophysics 213, 341–352.

Patrascu, S., Panaiotu, C., Secleman, M., Panaiotu, C.E., 1994. Timing of rotational motion of Apuseni Mountains (Romania): paleomagnetic data from Tertiary magmatic rocks. Tectonophysics 233, 163–176.

Pollard, D.D., Saltzer, S.D., Rubin, A.M., 1993. Stress inversion methods: are they based on faulty assumptions? J. Struct. Geol. 15 (8), 1045–1054.

Rabagia, T., Fülop, A., 1994. Syntectonic sedimentation history in the Southern Carpathians foredeep. In: Berza, T. (Ed.), Geological evolution of the Alpine–Carpathian–Pannonian system, ALCAPA II, field guidebook, Rom. J. Tect. Reg. Geol., 48.

Rabagia, T., Matenco, L., 1999. Tertiary tectonic and sedimentological evolution of the South Carpathians foredeep: tectonic versus eustatic control. Marine Petrol. Geol. in press.

Ratschbacher, L., Linzer, H.G., Moser, F., Strusievicz, R.O., Bedelean, H., Har, N., Mogos, P.A., 1993. Cretaceous to Miocene thrusting and wrenching along the central South Carpathians due to a corner effect during collision and orocline formation. Tectonics 12, 855–873.

Rögl, F., 1996. Stratigraphic correlation of Paratethys Oligocene and Miocene. Mitt. Ges. Geol. Bergbaustud. Österr. 41, 65–73.

Royden, L.H., 1988. Late Cenozoic Tectonics of the Pannonian Basin System. In: Royden, L.H., Horvath, F. (Eds.), The Pannonian Basin, A Study in Basin Evolution, AAPG Memoir., 27–48.

Sanders, C., 1998. Tectonics and erosion, competitive forces in a compressive orogen: a fission track study of the Romanian Carpathians. Ph.D. Thesis, Vrije Universiteit, Amsterdam, 204 pp.

Sandulescu, M., 1975. Essai de synthese structurale des Carpathes. Bull. Soc. Geol. Fr. XVII, 299.

Sandulescu, M., 1984. Geotectonica României. Ed. Tehnica, Bucharest. 450 pp. (in Romanian).

Sandulescu, M., 1988. Cenozoic Tectonic History of the Carpathians. In: Royden, L.H., Horvath, F. (Eds.), The Pannonian Basin, A Study in Basin Evolution, AAPG Memoir., 17–25.

Schmid, S.M., Berza, T., Diaconescu, V., Froitzheim, N., Fuegenschuh, B., 1998. Orogen-parallel extension in the South Carpathians during the Paleogene. Tectonophysics 297, 1–4, 209–228.

Seghedi, A., Berza, T., 1994. Duplex interpretation for the structure of the Danubian thrust sheets. Rom. J. Tect. Reg. Geol. 75, 57.

Simpson, C., Schmid, S.M., 1983. An evaluation of criteria to dedude the sense of movement in sheared rocks. Geol. Soc. Am. Bull. 94, 1281–1288.

Spang, J.H., 1972. Numerical method for dynamic analysis of calcite twin lamellae. Geol. Soc. Am. Bull. 83, 467–472.

Stan, N., Intorsureanu, I., Tiepac, I., Udrescu, C., 1992. Petrology of the Sichevita granotiods (South Carpathians). Rom. J. Petrol. 75, 183–188.

Stefanescu, M., working group 1988. Geological cross-sections at scale 1:200,000 no B1-6., Inst. Geol. Geofiz., Bucharest.

Streckeisen, A., 1934. Sur la tectonique des Carpathes Méridionales. An. Inst. Géol. 16, 327–481.

Turner, F.J., 1962. 'Compression' and 'tension' axes deduced from {0112} twinning in calcite. J. Geophys. Res. 67, 1660–1670.

Zweigel, P., 1997. The tertiary tectonic evolution of the Eastern Carpathians (Romania): orogenic arc formation in response to microplate movements. Ph.D. Thesis, Tubinger Geowissenschaftliche Arbeiten, no. 33, 159 pp.

Zweigel, P., Ratschbacher, L., Frisch, W., 1998. Kinematics of an arcuate fold–thrust belt: the southern East Carpathians (Romania). Tectonophysics 297, 1–4, 177–207.

Wallbrecher, E., 1986. Tektonische und gefugeanalytische Arbeitsweisen. Stuttgart. 224 pp.